A moonlighting function of Atg11 in spindle positioning

Md. Hashim Reza[1], Rashi Aggarwal[1#], Jigyasa Verma[1$#], Ratul Chowdhury[2], Ravi Manjithaya[3], and Kaustuv Sanyal[1*]

[1]Molecular Mycology Laboratory, Molecular Biology and Genetics Unit, Jawaharlal Nehru Centre for Advanced Scientific Research, Jakkur, Bangalore 560 064, India.

[2]Department of Systems Biology, Harvard Medical School, Boston, MA 02115, USA.

[3]Autophagy Laboratory, Molecular Biology and Genetics Unit, Jawaharlal Nehru Centre for Advanced Scientific Research, Jakkur, Bangalore 560 064, India.

*Corresponding author: Molecular Mycology Laboratory, Molecular Biology and Genetics Unit, Jawaharlal Nehru Centre for Advanced Scientific Research, Jakkur, Bangalore 560 064, India. Phone: +91 80 2208 2878, e-mail: sanyal@jncasr.ac.in

[#]These authors contributed equally: Rashi Aggarwal, Jigyasa Verma

[$]Present address: Department of Cellular and Physiological Sciences, University of British Columbia, Vancouver, BC, V6T1Z3, Canada.

Keywords: chromosome segregation, selective autophagy, astral microtubules, spindle position checkpoint (SPOC), spindle assembly checkpoint (SAC), SPB asymmetry, asymmetric cell division, chromosome loss, budding yeast, kinetochore

Abstract

Autophagy is an evolutionarily conserved degradation mechanism of misfolded proteins and damaged organelles which helps maintain cellular homeostasis. Besides its canonical function, proteins of the autophagy pathway also participate in other cellular processes including chromosome congression. Here, we perform a comprehensive screen of autophagy mutants in yeast and found that cells lacking an autophagy-related protein Atg11 have poor mitotic stability of linear and circular chromosomes. *atg11*Δ cells grow slowly at 37°C and accumulate at metaphase with aberrant astral microtubules (aMTs) along with mispositioned and misaligned spindles. Deletion of the spindle positioning checkpoint (SPOC) factor Bub2, but not the spindle assembly checkpoint (SAC) component Mad2, could improve the growth of the *atg11*Δ cells. Strikingly, the spindle pole body (SPB) localization pattern of an SPB component Spc72 is found to be randomized in *atg11*Δ cells resulting in inverted SPB inheritance. Atg11 is transiently localized to SPBs and interacts both physically and genetically with Spc72. Taken together, our study uncovers a moonlighting function of Atg11 participating between spatially separated processes, the cell cycle and autophagy, essential for proper spindle positioning and asymmetric SPB inheritance. Our findings, therefore, highlight one of the many failsafe mechanisms likely in place to ensure asymmetric cell division.

Introduction

Saccharomyces cerevisiae and related budding yeasts have intact nuclear envelope throughout the cell cycle (Byers, 1981; De Souza & Osmani, 2007; Heath, 1980; Thakur & Sanyal, 2012). Spindle pole bodies (SPBs), the microtubule organizing centers (MTOCs), in these organisms remain embedded in the nuclear envelope throughout the cell cycle (Fu, Hagan, & Glover, 2015). SPBs emanate both nuclear and cytoplasmic or astral microtubules (aMTs). Microtubules (MTs) emanating from the nuclear side of the SPBs that attach to kinetochores facilitate the poleward movement of sister chromatids required for precise segregation of chromosomes in the daughter cells. Defects in MT attachments or improper tension at the kinetochore are sensed by the spindle assembly checkpoint (SAC), which halts the cell cycle at metaphase until all the errors are corrected (Lara-Gonzalez, Pines, & Desai, 2021; Musacchio & Salmon, 2007). On the other hand, the cytosolic face of the SPBs nucleates aMTs which aid in the alignment and positioning of the mitotic spindle along the polarity axis, critical for proper nuclear division during asymmetric cell division in *S. cerevisiae*. Misaligned spindles lead to the activation of the spindle position checkpoint (SPOC) (Bloecher, Venturi, & Tatchell, 2000; Nelson, Sanson, Park, & Cooper, 2012; Pereira, Hofken, Grindlay, Manson, & Schiebel, 2000; Wang, Hu, & Elledge, 2000; Yeh, Skibbens, Cheng, Salmon, & Bloom, 1995), a surveillance mechanism that halts the cell cycle and prevents exit from mitosis by inhibiting the mitotic exit network (MEN) signalling pathway (Caydasi, Ibrahim, & Pereira, 2010).

In budding yeast, the spatial crosstalk between asymmetric nucleation of aMTs and cortical cues regulating the mitotic spindle alignment along the polarity axis requires the action of two functionally redundant pathways (Korinek, Copeland, Chaudhuri, & Chant, 2000; L. Lee et al., 2000; Miller, Cheng, & Rose, 2000; Segal & Bloom, 2001; Yeh et al., 1995). Two different premises suggest that the aMT asymmetry at the SPBs stems from the contribution of extrinsic and intrinsic factors (Geymonat et al., 2020). Kar9, present at both poles during the onset of SPB separation, represents the extrinsic control of the aMT asymmetry (Lengefeld & Barral, 2018). It gets phosphorylated only at newly formed SPB at the mother bud (mSPB), but not at the pre-existing old SPB that is located at the daughter bud (dSPB), by Cdk1/Clb4 and thus displays asymmetric SPB localization (Liakopoulos, Kusch, Grava, Vogel, & Barral, 2003). On the other hand, the cyclin-dependent kinase (CDK) Cdc28/Cdk1, representing the intrinsic factor, facilitates the biased recruitment of SPB components such as Spc72 and the γ-tubulin complex (γ-TC) at the old SPB (dSPB) during the early cell cycle. Subsequently, this facilitates the assembly of the new SPB (mSPB) in the correct order with the recruitment of the

outer plaque following the complete assembly of the inner plaque (Geymonat et al., 2020). Such asymmetry leads to the nucleation of aMTs from the dSPB necessary for the mitotic spindle positioning along the mother-bud axis (Markus, Kalutkiewicz, & Lee, 2012; Palmer, Sullivan, Huffaker, & Koshland, 1992; Shaw, Yeh, Maddox, Salmon, & Bloom, 1997; Sullivan & Huffaker, 1992). Any perturbations in MT dynamics lead to an improper spindle alignment and consequently asymmetric cell division which has wide implications ranging from failure in embryonic development, early ageing, aneuploidy and cancer (Cheng et al., 2008; Knoblich, 2010; Lancaster & Knoblich, 2012; Manzano-Lopez, Matellan, Alvarez-Llamas, Blanco-Mira, & Monje-Casas, 2019; Yamashita, Mahowald, Perlin, & Fuller, 2007). Therefore, it is imperative to identify new factors determining asymmetric cell division by preserving aMT integrity and spindle positioning.

Autophagy, apart from being a conserved cellular degradation process, is also implicated in cell division under stress conditions (Dotiwala et al., 2013; Matsui, Kamada, & Matsuura, 2013) and in controlling the integrity of nuclear-envelope-embedded nuclear pore complexes during cell cycle (C. W. Lee et al., 2020; Shcheprova, Baldi, Frei, Gonnet, & Barral, 2008). A series of emerging evidence has also highlighted the role of autophagy in cell metabolism, growth, ageing, and genome stability (Dotiwala et al., 2013; Matsui et al., 2013; Vessoni, Filippi-Chiela, Menck, & Lenz, 2013). In this study, we identified Atg11 from a collection of autophagy mutants as a regulator of high-fidelity chromosome segregation in *S. cerevisiae*. Under stress and starvation conditions, autophagy is induced and involves Atg17-meditated non-selective degradation of cargoes, while Atg11 mediates selective autophagy predominantly under vegetative conditions (Matscheko, Mayrhofer, Rao, Beier, & Wollert, 2019). Our results uncover previously unknown roles of Atg11 in regulating asymmetric SPB inheritance and aMT integrity vital for proper spindle alignment and positioning during mitosis.

Results

Atg11 plays an autophagy-independent role in high-fidelity chromosome transmission by facilitating timely anaphase onset

We carried out a phenotypic screen to determine the growth fitness of null mutants of autophagy (*atg*) in *S. cerevisiae* to a microtubule depolymerizing drug thiabendazole (TBZ). Among all the 35 *atg* mutants (**Figure 1-figure supplement 1A**), *atg11*Δ cells displayed maximum sensitivity to TBZ (**Figure 1A**), supporting an earlier observation (Strome, Wu, Kimmel, & Plon, 2008). Transgenic wild-type *ATG11* complemented the TBZ-induced growth defects in *atg11*Δ cells (**Figure 1A**). Furthermore, *atg11*Δ cells displayed a slow growth at

37°C (**Figure 1B**), a condition at which the rate of depolymerization of microtubules is more prominent than the rate of polymerization (Li & Moore, 2020). We conclude a specific role of Atg11 in regulating MT-dependent processes.

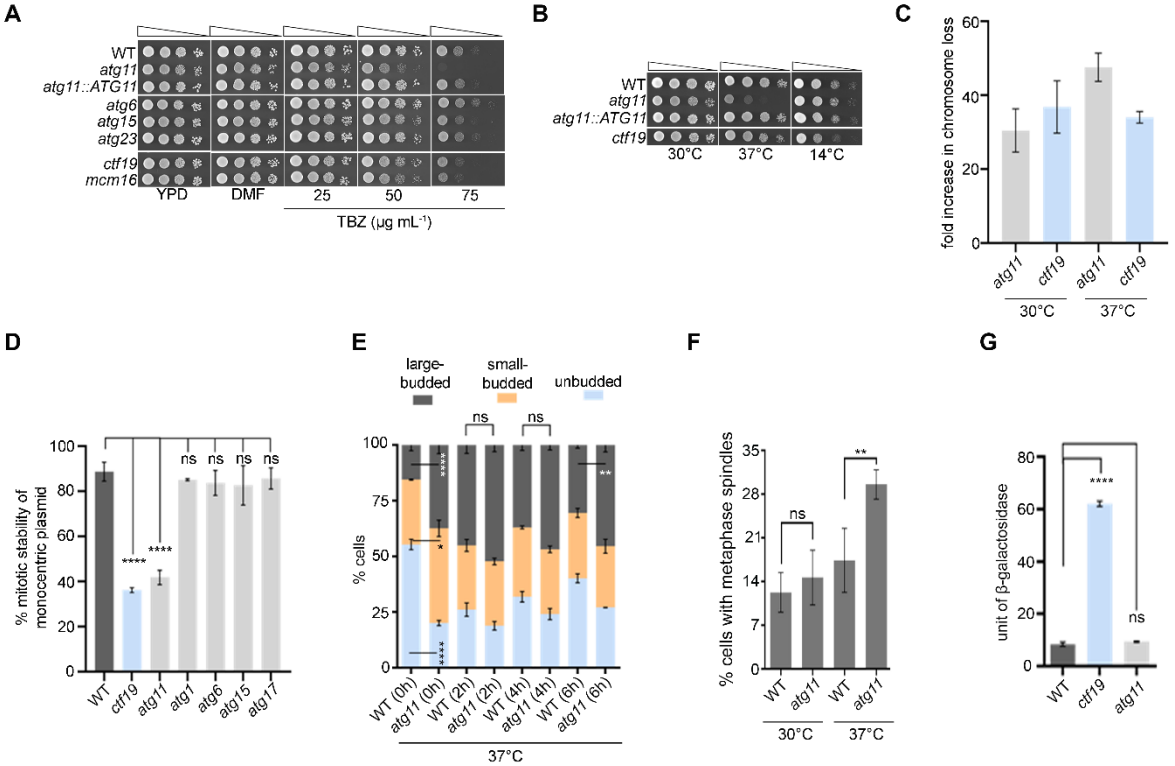

Figure 1. Cells lacking Atg11 show an increased rate of chromosome loss and delayed anaphase onset. (A) Overnight grown cells of wild-type (WT), autophagy (*atg*) mutants, and kinetochore mutants *ctf19*Δ and *mcm16*Δ were 10-fold serially diluted, spotted on YPD and YPD plates containing dimethylformamide (DMF) or increasing concentration of thiabendazole (TBZ) as indicated. Plates were photographed after incubation at 30°C for 2 days. (B) Overnight grown cells of indicated strains were 10-fold serially diluted and spotted on YPD plates. Plates were photographed after incubation at 30°C and 37°C for 2 days, or 14°C for 7 days. (C) Bar graph showing fold increase in chromosome loss in *atg11*Δ and *ctf19*Δ strains at 30°C and 37°C. Error bars indicate standard deviation (SD). (D) Mitotic stability of a monocentric plasmid (pRS313) was determined in wild-type, autophagy (*atg*) mutants as indicated, as well as in the kinetochore mutant strain *ctf19*Δ. The assay was done with three independent sets of transformants. Statistical analysis was done using one-way ANOVA using Dunnett's multiple comparisons tests (****$p<0.0001$). (E) Bar graph representing the proportion of unbudded, small-budded, and large-budded cells in wild-type (WT) and *atg11*Δ cells grown in YPD for 0, 2, 4, and 6 h at 37°C. More than 100 cells were analyzed for each biological replicate and for every time point, N=3. Error bars show mean ± SEM. Statistical analysis was done by two-way ANOVA using Tukey's multiple comparisons test (*$p=0.0128/0.0451$, ****$p<0.0001$). (F) A bar graph representing the percent large-budded cells having metaphase (1-2 µm) spindle (GFP-Tub1) in wild-type and *atg11*Δ cells at 30°C and 37°C. $n>89$, N=3. Error bars show mean ± SEM. Statistical analysis was done by one-way ANOVA using Tukey's multiple comparisons test at $p<0.05$. (G) Bar graph representing β-galactosidase levels of the corresponding strains. The measurement was performed in

triplicates. Statistical analysis was done by one-way ANOVA using Dunnett's multiple comparisons test ($p<0.0001$).

Any defects in MT-dependent processes negatively impact the fidelity of chromosome segregation. Indeed, a strain harboring an extra linear chromosome displayed a significantly higher rate of chromosome loss in *atg11*Δ cells at 30°C that was further exacerbated at 37°C (**Figure 1C**). Similarly, the average mitotic stability of a monocentric circular plasmid was found to be significantly lower in *atg11*Δ cells than in the wild-type but comparable to that of a kinetochore mutant, *ctf19*Δ (**Figure 1D**). No other *atg* mutants tested displayed any decrease in the mitotic plasmid stability. Mutants of key autophagy proteins such as Atg1, essential for both cytoplasm-to-vacuole targeting (Cvt) and autophagy pathways, or Atg17, required during starvation (Kim et al., 2001), neither displayed any TBZ sensitivity nor any drop in plasmid stability (**Figure 1D**). Hence, we conclude that the role of Atg11 in mediating error-free chromosome segregation is independent of its autophagy function. Further analysis showed that the overnight grown (0 h) *atg11*Δ cells displayed a significantly increased proportion of large-budded cells compared to wild-type (**Figure 1E**). When grown at 37°C for 6 h, the *atg11*Δ cells further accumulated an increased proportion of large-budded cells (**Figure 1E**), with a two-fold higher proportion of large-budded cells with metaphase spindle of 1-2 µm compared to the wild-type at 37°C (**Figure 1F**), hinting towards a delay in anaphase onset. The *CEN* transcriptional read-through assay ruled out the role of Atg11 in the maintenance of the kinetochore ensemble (**Figure 1G** and **Figure 1-figure supplement 1B**). Thus, we, conclude that the loss of Atg11 perturbs MT-dependent processes leading to a delay in anaphase onset.

Atg11-mediated maintenance of aMT integrity is crucial for proper spindle positioning

To examine the dynamics of MTs, we performed live-cell imaging of GFP-tagged mitotic spindle and found a significant delay in cell cycle progression in *atg11*Δ cells (**Figure 2A-C**). Strikingly, *atg11*Δ cells displayed short and unstable aMTs (**Figure 2A-B** and **Figure 2-figure supplement 1A-B**).

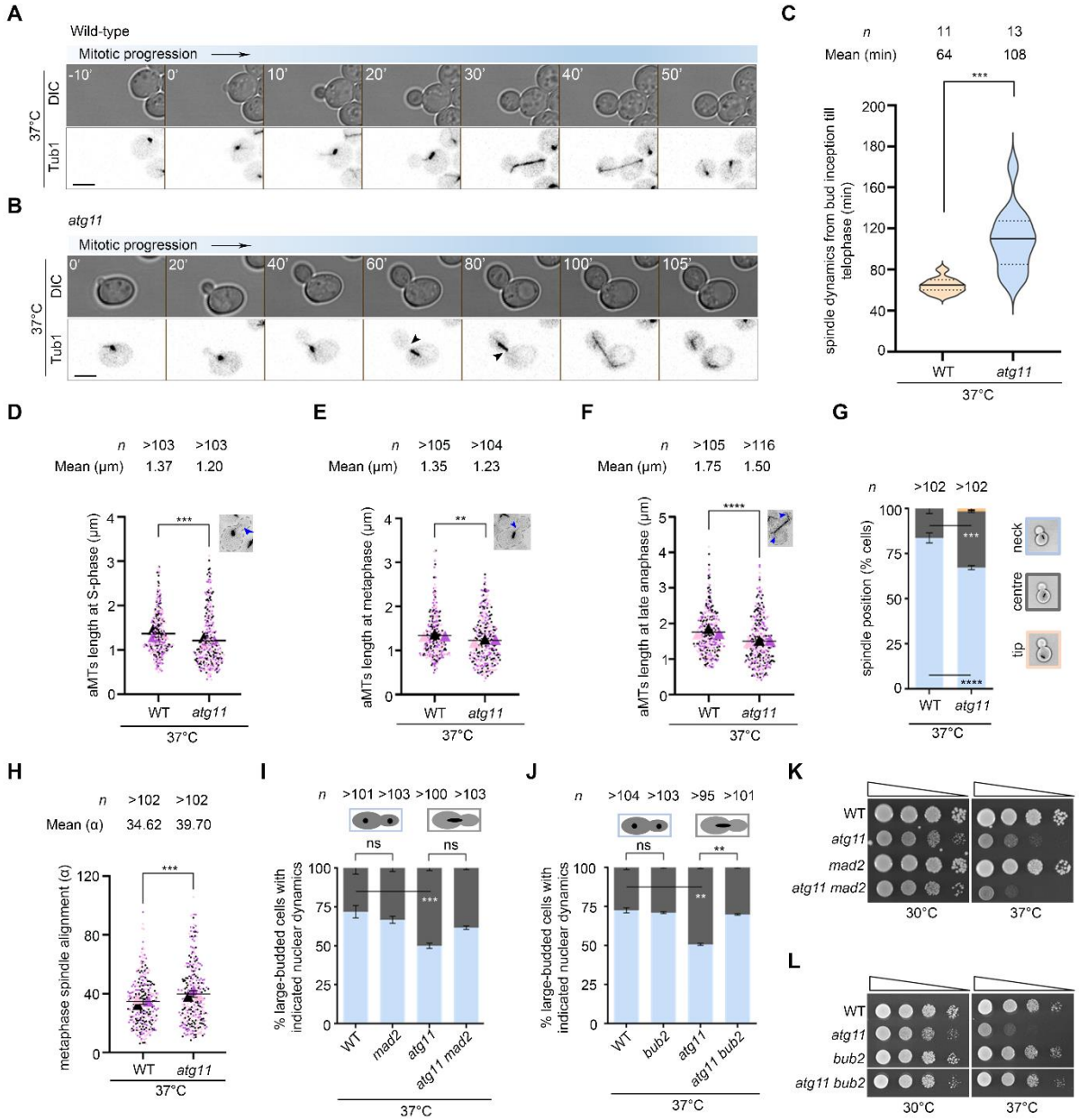

Figure 2. The delayed anaphase onset in *atg11*Δ cells is Bub2-mediated which results in the accumulation of cells with shorter astral MTs. Time-lapse images showing spindle (GFP-Tub1) dynamics during cell cycle in (A) wild-type and (B) *atg11*Δ cells at 37°C. Scale bar, 5 µm. aMTs could not be detected (black arrowheads) in *atg11*Δ cells at 60 and 80 min. (C) A violin plot displaying the time taken for the disappearance of the mitotic spindle from the inception of bud in strains as indicated at 37°C. The number on top represents the average time taken for the process indicated. *n*, number of live-cell movies analyzed. The solid line on the violin plot represents the median value, while the dotted lines represent quartiles. The statistical significance was done using an unpaired *t*-test with Welch's correction (***p=0.0002). The aMT length was measured in (D) S-phase (<1 µm mitotic spindle), (E) metaphase (1-2 µm mitotic spindle), and (F) late anaphase (>7 µm mitotic spindle) in wild-type (WT) and *atg11*Δ cells grown at 37°C. A representative image for each stage is shown along the *y*-axis. aMTs are marked with blue arrowheads. *n*, a minimum number of cells analyzed, N=3. The statistical significance was done using an unpaired *t*-test with Welch's correction (**p=0.0054, ***p=0.0003, ****p<0.0001). (G) The metaphase cells of wild-type (WT) and *atg11*Δ cells grown at 37°C were analyzed for the position of the short bipolar

spindle. *n*, a minimum number of cells analyzed, N=3. Statistical analysis was done by two-way ANOVA using Sidak's multiple comparison test (***p=0.0001 and ****p<0.0001). (H) The metaphase cells of wild-type (WT) and *atg11*Δ cells grown at 37°C and displaying a short bipolar spindle were analyzed for the angle of alignment along the mother-bud axis. *n*, a minimum number of cells analyzed, N=3. The statistical significance was done using an unpaired *t*-test with Welch's correction (***p=0.0007). (I) Bar graph representing the percent large-budded cells with stages of nuclear division in indicated strains when grown at 37°C. Error bars show mean ± SEM. Cartoons represent cellular morphology (grey), and chromatin mass (black) associated with the corresponding class. *n*, a minimum number of cells analyzed, N=3. Statistical analysis was done by two-way ANOVA using Tukey's multiple comparisons test (***p=0.0002). (J) Bar graph representing the percent large-budded cells (budding index >0.6) with stages of nuclear division in indicated strains when grown at 37°C. Error bars show mean ± SEM. Cartoons represent cellular morphology (grey), and chromatin mass (black) associated with the corresponding class. *n*, a minimum number of cells analyzed, N=3. Statistical analysis was done by two-way ANOVA using Tukey's multiple comparisons test (**p=0.0024/0.0023). (K) Overnight grown cells of wild-type, single and double mutants were 10-fold serially diluted and spotted on YPD at 30°C and 37°C. Plates were photographed after 48 h of incubation. (L) Overnight grown cells of wild-type, single and double mutants were 10-fold serially diluted and spotted on YPD at 30°C and 37°C. Plates were photographed after 33 h of incubation.

To assess the difference, we, therefore measured the length of aMTs at S-phase, metaphase, and late anaphase and found that *atg11*Δ cells displayed significantly shorter aMTs at all three stages of the cell cycle (**Figure 2D-F** and **Figure 2-figure supplement 1C-E**). Mutants that display shorter aMTs also show a defective orientation and positioning of the mitotic spindle, thereby highlighting the importance of aMTs in these processes (Cottingham & Hoyt, 1997; DeZwaan, Ellingson, Pellman, & Roof, 1997; Hoepfner, Schaerer, Brachat, Wach, & Philippsen, 2002; Kosco et al., 2001; Matellan, Manzano-Lopez, & Monje-Casas, 2020; Soues & Adams, 1998; Tirnauer, O'Toole, Berrueta, Bierer, & Pellman, 1999). Therefore, we scored these defects in the *atg11*Δ cells. Indeed, *atg11*Δ cells displayed a two-fold increase in the proportion of cells having a metaphase spindle at the central region in the mother cell (**Figure 2G** and **Figure 2-figure supplement 1F**), as well as a significantly higher angle of alignment of the metaphase spindle than wild-type (**Figure 2H** and **Figure 2-figure supplement 1G**).

In response to spindle damage, *S. cerevisiae* is known to employ two independent surveillance mechanisms, SAC and SPOC to delay metaphase-to-anaphase transition (Alexandru, Zachariae, Schleiffer, & Nasmyth, 1999; Fraschini, Formenti, Lucchini, & Piatti, 1999). We, therefore, asked whether the *atg11*Δ-associated defects were monitored by either of these mitotic checkpoints. Deletion of *MAD2* in the *atg11*Δ cells did not alleviate the proportion of large-budded cells with unsegregated nuclei (**Figure 2I** and **Figure 2-figure**

supplement 1H), whereas, deletion of *BUB2* rescued the proportion of large-budded cells with unsegregated nuclei along with the slow growth phenotype of *atg11*Δ cells (**Figure 2J-L** and **Figure 2-figure supplement 1I**). SPOC-mediated delay in anaphase onset in *atg11*Δ cells was further confirmed by the appearance of 4N population in both *bub2*Δ cells and *atg11*Δ *bub2*Δ double mutant upon treatment with MT poison (**Figure 2-figure supplement 1J**). Cdc5, a polo-like kinase, functions upstream of Bfa1-Bub2 (Hu et al., 2001; Ro, Song, & Lee, 2002). Rescue of growth defects of *atg11*Δ cells in the *atg11*Δ *bub2*Δ double mutant is comparable to the double mutants of *cdc5-1 bub2*Δ and *cdc5-2 bub2*Δ (Hu et al., 2001; Ro et al., 2002), suggesting that like Cdc5, Atg11 also functions upstream of Bub2. These results demonstrate that the SPOC-mediated delay in anaphase onset observed in *atg11*Δ cells is due to defective spindle positioning caused by shorter aMTs.

Atg11 ensures proper SPB inheritance by maintaining the asymmetric distribution of Spc72 at the SPBs

The asymmetric localization of Kar9 at the dSPB determines non-random SPB inheritance during cell cycle (Liakopoulos et al., 2003). Proper integrity of aMTs ensures the asymmetric inheritance of the old SPB into the daughter bud (Pereira, Tanaka, Nasmyth, & Schiebel, 2001) (**Figure 3A**).

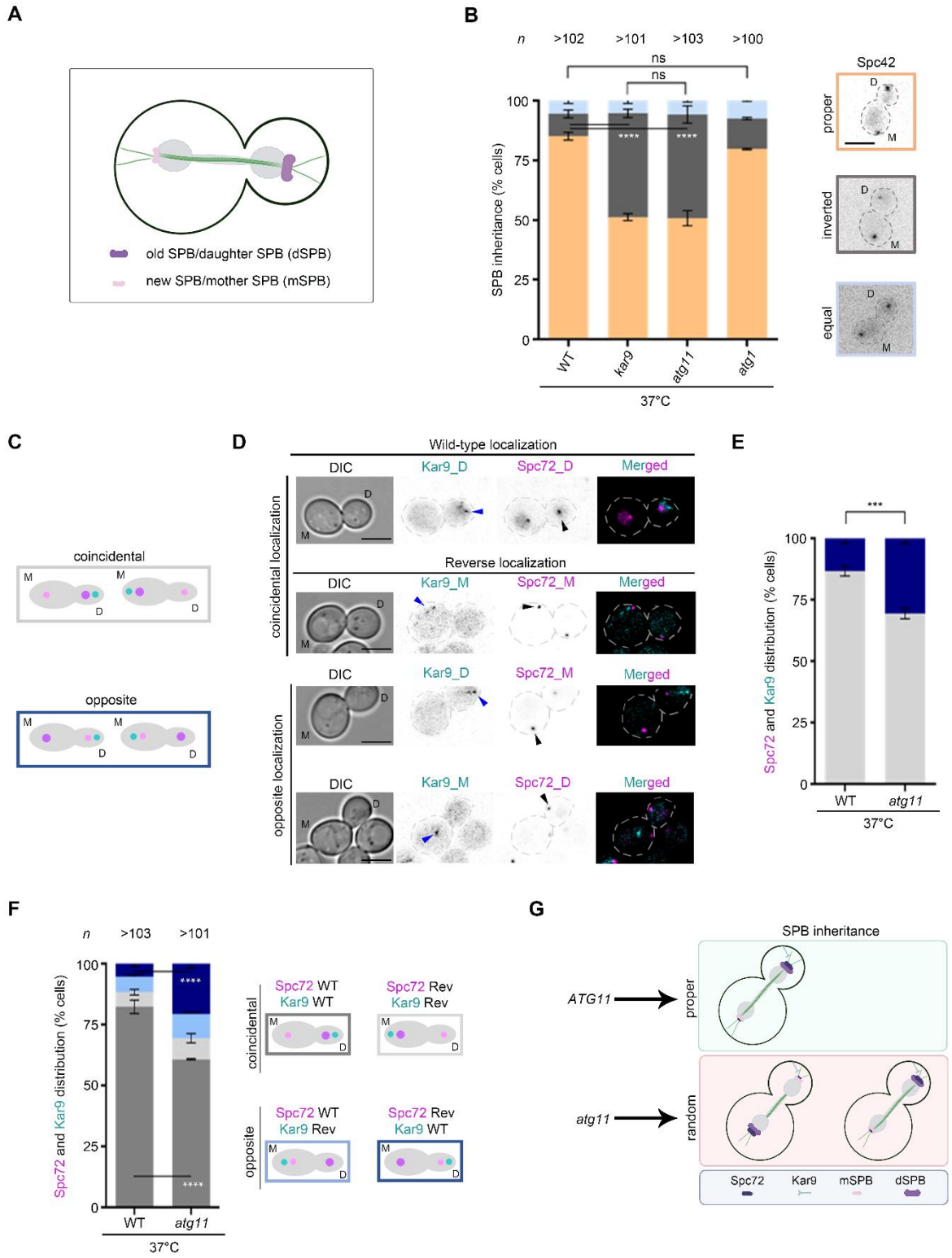

Figure 3. *atg11*Δ cells exhibit SPB inheritance defects due to inverted SPB localization of Spc72 and Kar9. (A) Schematic showing proper SPB inheritance in budding yeast. The old SPB with more preassembled proteins segregates into the daughter cell and hence is also referred to as daughter SPB (dSPB), while the new SPB with *de novo* assembly of proteins is retained in the mother cell and is called mother SPB (mSPB). (B) A bar graph displaying percent cells having proper (old SPB in the daughter cell), reversed (old SPB in the mother cell), or symmetric (SPBs are indistinguishable) SPB inheritance in the indicated strains based

on the Spc42-mCherry signal intensity at 37°C. *Right*, representative images of above mentioned SPB inheritance are shown. M and D represent the mother and daughter cells respectively. *n*, a minimum number of cells analyzed, N=3. Statistical analysis was done by two-way ANOVA using Dunnett's multiple comparisons test (****p<0.0001). Scale bar, 5 µm. (C) Schematic representation displaying coincidental or opposite distribution of Spc72 and Kar9 in budding yeast. (D) Representative images displaying coincidental or opposite distribution of Kar9 (cyan) and Spc72 (magenta) in wild-type (WT) and *atg11*Δ cells, exhibiting wild-type-like asymmetric and predominant accumulation of both the proteins in the daughter bud (D) or reversed such that asymmetric and predominant accumulation of these proteins in the mother (M) cell. Asymmetric localization of Kar9-GFP and Spc72-mCherry is marked by blue and black arrowheads respectively. Scale bar, 5 µm. (E) Bar graph representing the percent of cells displaying coincidental (light grey) and opposite (dark blue) Kar9-GFP and Spc72-mCherry SPB localization at 37°C. (F) For coincidental and opposite Kar9 and Spc72 localization, the wild-type and reversed distribution patterns are further subclassified and represented as the percent of cells in the bar graph. *n*, a minimum number of cells analyzed, N=3. Error bars show mean ± standard error of mean (SEM). Statistical analysis was done by two-way ANOVA using Sidak's multiple comparison test (***p=0.0004 and ****p<0.0001). (G) Schematic displaying the role of Atg11 in asymmetric localization of Spc72 at SPBs facilitating predetermined SPB inheritance in budding yeast.

Having shown shorter aMTs with loss of Atg11, we asked whether *atg11*Δ cells display any defects in SPB inheritance. To test the hypothesis, we tagged Spc42 (SPB marker) with mCherry. The slow folding kinetics of mCherry and ordered assembly of SPB allow age discrimination with the new SPB being much dimmer than the old SPB (Manzano-Lopez et al., 2019). Deletion of *KAR9*, known to display random SPB inheritance (Pereira et al., 2001), led to a randomized SPB inheritance relative to the wild-type (**Figure 3B** and **Figure 3-figure supplement 1A**). Strikingly, *atg11*Δ cells displayed a four-fold increase in SPB inheritance defects (**Figure 3B** and **Figure 3-figure supplement 1A**). Notably, the loss of a key autophagy protein, Atg1 segregated the SPBs similar to the wild-type (**Figure 3B** and **Figure Figure 3-figure supplement 1A**), further confirming that the role of Atg11 in SPB inheritance is autophagy-independent.

A previous report on the localization interdependency of Spc72 and Kar9 onto the SPBs, placed Spc72 upstream of Kar9 (Juanes et al., 2013), while a recent study demonstrates Cdc5 as a molecular timer facilitating timely recruitment of both Spc72 and Kar9 onto the SPBs (Matellan et al., 2020). Based on the SPB inheritance defects, we asked whether Atg11 contributes to the asymmetric localization of Spc72 and Kar9 at the SPBs. While wild-type cells display asymmetric localization of both Spc72 and Kar9 at the dSPB (coincidental localization), Cdc5 inhibition leads to asymmetric localization of either Spc72 or Kar9 at the mSPB (opposite localization) (Matellan et al., 2020). Like Cdc5 inhibition, *ATG11* deletion randomized the loading of Spc72 and Kar9 on SPBs (**Figure 3C-E**), as judged by a

significantly increased proportion of cells having opposite localization patterns of Spc72 and Kar9 on SPBs (**Figure 3E** and **Figure 3-figure supplement 1B**). Interestingly, loss of *ATG11* randomized the SPB localization of Spc72 even when Kar9 was properly and asymmetrically localized in the daughter bud (**Figure 3F** and **Figure 3-figure supplement 1C**), suggesting that Atg11 is specific in maintaining the asymmetric Spc72 localization at the dSPB (**Figure 3G**).

Atg11 genetically interacts with Spc72 to maintain the integrity of aMTs

With a loss in asymmetric localization of Spc72 leading to an increased SPB inheritance defect in *atg11*Δ cells, we asked whether Atg11 is associated with the SPBs during the cell cycle. Using a strain that expressed sfGFP-Atg11, we confirmed the canonical localization of Atg11 onto the vacuolar membrane as a punctate signal (**Figure 3-figure supplement 1D**) (Yorimitsu & Klionsky, 2005). Live-cell imaging of Atg11 and Spc42 during the cell cycle revealed proximal localization of Atg11 first with the old SPB (14 out of 15 live-cell movies) (**Figure 3-figure supplement 1E**), and then near the new SPB at a later stage (**Figure 3-figure supplement 1F**). Being an SPB component of the outer plaque, Spc72 mediates aMT nucleation, spindle elongation, nuclear migration and spindle positioning through Kar9, Myo2 and Bim1 (Beach, Thibodeaux, Maddox, Yeh, & Bloom, 2000; Chen, Yin, & Huffaker, 1998; Knop & Schiebel, 1998; Korinek et al., 2000; L. Lee et al., 2000; Soues & Adams, 1998; Yin, Pruyne, Huffaker, & Bretscher, 2000). Interestingly, Spc72 is identified as one of the key interactors of Atg11 from a protein-protein interaction network analysis of components involved in autophagy and chromosome segregation (**Figure 4A**) (Stark et al., 2006).

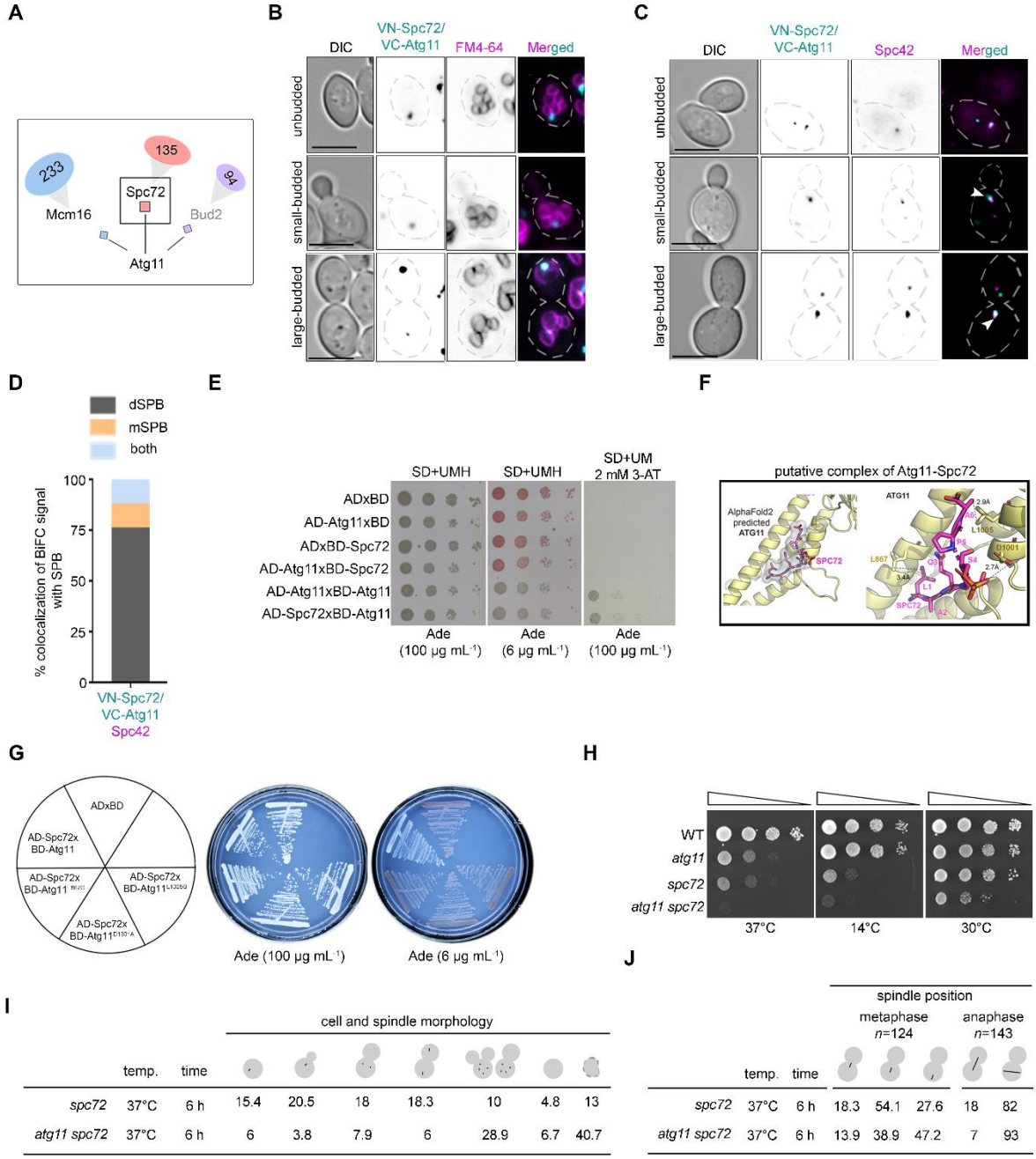

Figure 4. Atg11 directly interacts with Spc72 at SPBs to mediate proper spindle positioning. (A) Primary (square boxes) and secondary (oval) interactors of Atg11 as reported in the latest curation of BioGRID (Stark et al., 2006). (B) Representative images displaying an *in vivo* BiFC interaction between Atg11 and Spc72 by the reconstitution of Venus fluorescence (VN-Spc72 /VC-Atg11) in the diploid cells at the vacuolar periphery, marked by FM4-64 staining. Scale bar, 6 µm. (C) Representative images displaying an *in vivo* BiFC interaction between Atg11 and Spc72 at the SPBs, (Spc42-mCherry), in the diploid cells. The white arrowheads mark the co-localization of the BiFC signal with the dSPB. Scale bar, 6 µm. (D) A bar graph displaying the proportion of cells having colocalization of BiFC signals with either dSPB, mSPB, or both the SPBs (*n*=85 large-budded cells). (E) Yeast-two hybrid (Y2H) assays in *S. cerevisiae* strains carrying indicated plasmids were 10-fold serially diluted and spotted on SD - trp - leu or SD - trp - leu - his supplemented with 2 mM 3-amino-1,2,4-triazole (3-AT)

and grown at 30°C. (F) The putative complex of Atg11 and Spc72 is predicted using AlphaFold2 pipeline (Jumper et al., 2021). The flexible protein-protein docking with hexapeptide Spc72, which is held in place by hydrophobic packing of both the N-terminal and C-terminal residues, and electrostatic stabilization of the post-translationally modified Ser4 residue on Spc72 was performed. (G) Schematic displaying a yeast-two hybrid (Y2H) assay in *S. cerevisiae* transformants carrying plasmids as mentioned. The indicated strains expressing either the wild-type version of Atg11 or the point mutant versions of it along with Spc72 were streaked on SD - trp - leu and supplemented with 100 µg mL^{-1} adenine or 6 µg mL^{-1} adenine and grown at 30°C for 48 h. (H) Overnight grown cells of indicated strains were 10-fold serially diluted and spotted on YPD plates. Plates were photographed after 2 days of incubation at 30°C or 37°C, and 8 days at 14°C. (I) Various cellular morphology in *spc72*Δ and *atg11*Δ *spc72*Δ cells tagged with GFP-Tub1 and grown at 37°C for 6 h. The table shows the percentage of cells with a given cellular morphology along with mitotic spindles (unbudded, small-budded, and large-budded cells) from two independent biological repeats (*n*=399 cells). The deformed unbudded cell, outlined by the dashed line, represents a dead cell. (J) Metaphase and anaphase spindle positioning in large-budded cells of *spc72*Δ and *atg11*Δ *spc72*Δ tagged with GFP-Tub1 and grown at 37°C for 6 h. The table shows the percentage of cells with mitotic spindles in metaphase or anaphase at indicated positions from two independent biological experiments. *n*, a minimum number of cells analyzed.

To strengthen our observation of a transient and proximal localization of Atg11 with the SPBs, we utilized proximity-based bimolecular fluorescence complementation (BiFC) assay (Sung & Huh, 2007). A fluorescent punctate signal resulting from the reconstitution of the Venus molecule at the vacuolar periphery, marked by FM4-64, suggested an *in vivo* interaction between Atg11 and Spc72 (**Figure 4B**). Co-localization with Spc42 further demonstrated the *in vivo* interaction between these two proteins at the SPBs (**Figure 4C-D**). The absence of BiFC signal in diploid cells expressing either VN-tagged Spc72 or the VC-tagged Atg11 alone (**Figure 3-figure supplement 1G-H**), suggested that neither VN nor VC fluoresces on its own. Taken together, our results demonstrate that Atg11 is physically associated with the SPBs and mediates an autophagy-independent role in SPB inheritance.

To probe how Atg11 is associated with SPBs, we first confirmed a previously reported interaction between Atg11 and Spc72 (Wang et al., 2012) by the yeast two-hybrid (Y2H) assay (**Figure 4E**). The Y2H assay with Cnm67, a protein from the outer plaque of the SPB, did not show any interactions with Atg11 (**Figure 3-figure supplement 1I-J**), suggesting the spatial position of Atg11 and Spc72 favours their physical interactions. A flexible protein-protein docking study of Atg11 and Spc72 predicted hydrophobic packing of the peptide termini by Leu867 and Leu1005 residues of Atg11, and electrostatic stabilization of the phosphate group using the positively charged side chain of Asp1001 of Atg11 necessary for the Atg11-Spc72 interaction (**Figure 4F**). Y2H assay with Atg11 point mutants, L867G, L1005G, and D1001A

abrogated the interaction between Atg11 and Spc72 (**Figure 4G**), demonstrating the essentiality of these residues for the Atg11-Spc72 interaction.

Loss of Spc72 leads to defective nuclear positioning and spindle orientation and randomized SPB inheritance (Hoepfner et al., 2002; Matellan et al., 2020; Soues & Adams, 1998). Our results so far suggested similar defects in the *atg11*Δ cells. Having established a direct Atg11-Spc72 interaction, we, therefore, asked if loss of Atg11 leads to a compromised function of Spc72. To test this, we investigated whether combining the two mutations aggravates the *spc72*Δ defects. Indeed, the *atg11*Δ *spc72*Δ double mutant showed synthetic lethality at 37°C, synthetic sickness at 14°C and a significant growth defect at 30°C (**Figure 4H**). The *atg11*Δ *spc72*Δ double mutant cells displayed a three-fold increase in the proportion of both multi-budded cells with multiple foci of broken microtubules and dead cells when compared to *spc72*Δ cells at 37°C (**Figure 4I**). Remarkably, in 82% of the large-budded *spc72*Δ cells, the anaphase spindle was mispositioned in the mother cell which increased to 93% in the *atg11*Δ *spc72*Δ double mutant (**Figure 4J**). Taken together, our results demonstrate that the interaction of Atg11 with Spc72 maintains aMT integrity crucial for proper spindle positioning and alignment and asymmetric SPB inheritance in budding yeast.

Discussion

Increasing evidence suggests the contribution of spindle orientation defects in human disease and cancer (Diaz-Horta et al., 2012; Doherty et al., 2012; Fischer et al., 2006; Lechler & Mapelli, 2021; Morrow, Underwood, Seldin, Hinnant, & Lechler, 2019; Zimdahl et al., 2014), reinforcing the role of mitotic spindle positioning in cell cycle regulation. Our results demonstrate that Atg11 contributes to genome stability by performing an autophagy-independent role in maintaining aMT integrity in collaboration with Spc72 in *S. cerevisiae*. Our results show that Atg11 plays a role in aMT integrity under conditions which perturb MT dynamics and integrity. Consistent with this, the *atg11*Δ cells showed misaligned and misoriented spindle and inverted SPB asymmetry at 37°C. We show that Atg11 is associated with the SPBs with the help of Spc72 and Atg11-Spc72 together maintaining proper spindle positioning in budding yeast.

Atg11, localizing close to the dSPB during the metaphase-to-anaphase transition, adds to the list of proteins localizing differentially to the dSPB in *S. cerevisiae*. Cell cycle-dependent regulators ensure the asymmetric distribution of proteins on the two SPBs (Bardin, Visintin, & Amon, 2000; Manzano-Lopez et al., 2019; Miller & Rose, 1998; Molk et al., 2004). As a consequence, the dSPB nucleates long aMTs, while the mSPB forms short aMTs facilitating

the asymmetric inheritance of SPBs (Lengefeld & Barral, 2018; Pereira et al., 2001; Shaw et al., 1997). Therefore, any perturbations in aMT integrity randomize SPB inheritance to the daughter cell (Pereira et al., 2001). Remarkably, *atg11*Δ cells display SPB inheritance defects along with a loss in cell viability at an elevated temperature similar to Cdc5, Spc72, Nud1, or MEN components (Hotz et al., 2012; Matellan et al., 2020; Soues & Adams, 1998). Atg11 regulating the dynamics of aMTs, thereby impacting spindle positioning and alignment represents the first example to our knowledge of an autophagy protein mediating an autophagy-independent role in high-fidelity chromosome segregation in budding yeast (**Figure 5**).

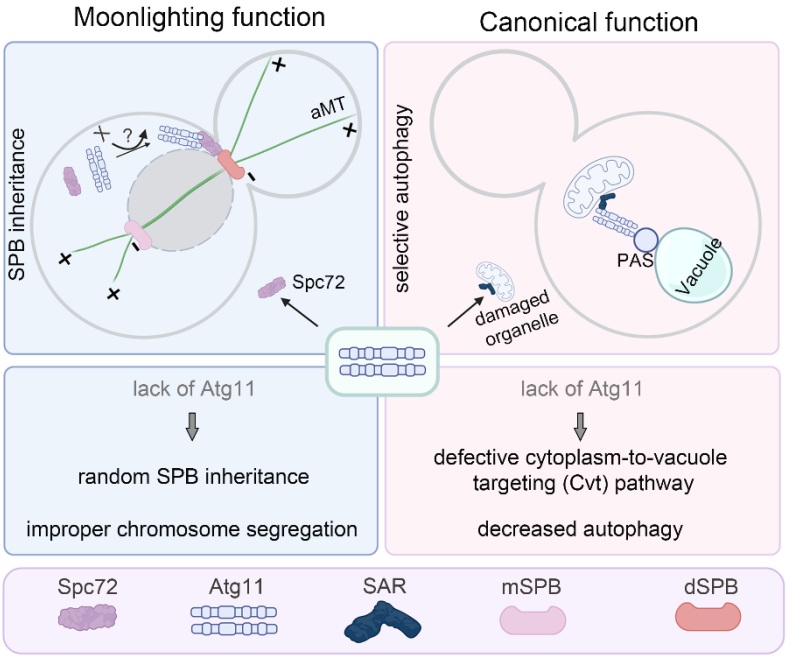

Figure 5. Atg11 regulates asymmetric SPB inheritance and astral microtubule dynamics to ensure high-fidelity chromosome segregation via an autophagy-independent pathway in yeast. A model summarizing both non-canonical moonlighting and canonical roles of Atg11 during cell cycle under nutrient-rich conditions. In the non-canonical role, Atg11 associates with SPBs by interacting directly with the Spc72 (purple), an SPB component present at the outer plaque and facilitates asymmetric localization of Spc72 at the dSPB (dark pink). It remains to be seen if Atg11 interacts with known/unknown regulators (X) to facilitate asymmetric SPB inheritance. Loss of Atg11 leads to shorter aMTs and as a result, contributes to spindle mispositioning of the mitotic spindle during metaphase. Lack of Atg11, as a consequence, results in the randomization of Spc72 localization, leading to SPB inheritance defects. Atg11 typically localizes at the pre-autophagosomal structures (PAS) onto the vacuolar membrane (Yorimitsu & Klionsky, 2005) and functions as a scaffold for PAS formation. Atg11 is vital for selective autophagy, wherein it interacts with specific autophagy receptors (SARs) present on damaged organelles. Loss of Atg11 leads to a defect in the Cvt vesicle formation (Shintani, Huang, Stromhaug, & Klionsky, 2002), defective pexophagy and mitophagy (Farre, Manjithaya, Mathewson, & Subramani, 2008; Mao, Wang, Liu, & Klionsky, 2013), and piecemeal microautophagy of the nucleus (Krick et al., 2008).

Furthermore, our results also uncover a genetic interaction with Atg11 and Spc72 in mediating aMT integrity. Like many known failsafe mechanisms, budding yeast also has robust mechanisms to correctly orient mitotic spindles even in the absence of stable aMTs. While the SPB half-bridge compensates for aMTs in *cnm67*Δ cells, the Kar3 motor helps reorient the mitotic spindle in *spc72*Δ cells (Brachat, Kilmartin, Wach, & Philippsen, 1998; Hoepfner et al., 2002). Synthetic lethality in the *atg11*Δ *spc72*Δ double mutant at 37°C even in the presence of Kar3, makes Kar3 dispensable and Atg11 essential under this condition. We, therefore, posit that Atg11 might play a role together with Kar3 and Spc72 in regulating aMT length crucial for proper spindle orientation.

Consisting of four coiled-coil domains, the fourth coiled-coil domain (CC4) of Atg11 is important for selective autophagy (**Figure 5**) (Yorimitsu & Klionsky, 2005). In the absence of the scaffolding role of Atg11 and Atg17, the function of the phagophore assembly site (PAS) is compromised. Additionally, during glucose-induced starvation, Atg11 is required for the PAS and Atg17 complex formation, Atg1 activity and recruitment of Atg9 vesicles (Yao et al., 2020). Albeit transiently, the emerging role of Atg11 being important for spindle positioning by interacting with Spc72, suggests a repurposing of the scaffolding function of Atg11 in budding yeast which undergoes closed mitosis. Remarkably, two of the three residues, crucial for Atg11-Spc72 interactions fall into the CC4 domain. Thus, it is likely that the CC4 domain is also important for the selective recognition and binding of Atg11 to Spc72 *in vivo*. We propose that being a bridging protein, Atg11 likely interacts, recruits, or positions proteins key for the asymmetric distribution of Spc72. Cdc5 physically interacts with Spc72 at dSPB during the metaphase-to-anaphase transition (Maekawa et al., 2017; Matellan et al., 2020) and facilitates the asymmetric localization of Kar9 (Matellan et al., 2020), crucial for regulating asymmetric SPB inheritance (Matellan et al., 2020; Moore, D'Silva, & Miller, 2006; Pereira et al., 2001). Since Cdc5 safeguards SPB asymmetry (Matellan et al., 2020), it is tempting to speculate that Atg11 and Cdc5 interact *in vivo* and such an interaction regulates SPB inheritance. It remains to be seen if Atg11 brings Cdc5 to dSPB or *vice-versa*. Furthermore, how loss-of-function of the CC4 domain of Atg11 affects the *in vivo* interaction with Spc72 and its consequence on the cell cycle progression remains an area of further investigation.

Our findings are significant in light of the autophagy-independent role of Beclin-1 in accurate kinetochore anchoring to the spindle during mitosis in cells undergoing open mitosis (Fremont et al., 2013). Thus, like Beclin-1, Atg11 could be another example of an autophagy protein performing a moonlighting function during cell cycle. It is likely that depending on the types of mitoses, the players might differ in performing a non-canonical function. More

examples of such non-canonical functions (Sreekumar et al., 2021; Varma et al., 2012), suggest how proteins organize between various processes to maintain cellular homeostasis. A series of evidence have established an interplay between errors in the spindle alignment with ageing and aneuploidy leading to the development of cancer and neurodegenerative diseases (Cheng et al., 2008; Knoblich, 2010; Lancaster & Knoblich, 2012; Manzano-Lopez et al., 2019; Yamashita et al., 2007). Likewise, perturbations in the autophagy function also contribute to various human diseases like neurodegenerative diseases, cancers, lysosomal storage disorders, and inflammatory disorders (Jiang & Mizushima, 2014; Mizushima & Levine, 2020). Our work adds to the importance of cellular functions carried out by transient protein-protein interactions vital for cellular fitness under specific conditions. Therefore, it becomes imperative to dissect these dynamic interactions essential for crosstalk between various biological processes.

Materials and Methods

Yeast strains, plasmids, and primers

All the strains used in this study are specified in Key Resources Table 1. Primer sequences and the plasmids used for strain construction are specified in Key Resources Table 2, and Key Resources Table 3 respectively.

Media and growth conditions

The yeast strains were grown on YPD media (yeast extract 1%, peptone 2%, and dextrose 2%) at 30°C unless stated otherwise. For the growth assay in presence of thiabendazole (TBZ), overnight grown cultures of wild-type, autophagy mutants, *ctf19*Δ, *mcm16*Δ, and *ATG11* complemented strains were serially diluted and spotted on YPD containing 50 µg mL^{-1} and imaged on 2 dpi or 36 h. The analyses for figures 1E, 2D-J, 3B, 3E-F, 4I-J, and supporting figures S2H-I were done by growing the cells at 37°C for 6 h.

Interaction network

We first constructed a protein-protein interaction map by identifying the proteins which have been reported to either genetically or physically interact with each of the Atg proteins. We further extended the network to include the proteins that are known to interact with any of the primary interactor proteins. We gleaned these connections using Perl scripts to query the latest curation of the BioGRID yeast interactomes (Stark et al., 2006). To this end, only those protein-protein interactions were retained which were confirmed and corroborated across three or more independent studies.

To discern the biophysical underpinnings of Atg11-Spc72 interactions, we set out to perform a flexible protein-protein docking using a ClusPro-type algorithm (Kozakov et al., 2017) within the OptMAVEn-2.0 docking protocol (Chowdhury, Allan, & Maranas, 2018). The Atg11 structure does not have experimentally validated crystallographic coordinates. Therefore, we predicted the structure using a deep multiple sequence alignment and fed it through the AlphaFold2 (AF2) pipeline (Jumper et al., 2021). The AF2-recommended MMSeq2 program (Steinegger & Soding, 2017) was first executed to obtain a deep multiple sequence alignment of the *Saccharomyces cerevisiae* Atg11 sequence against all known protein and metagenomic sequences (~270 M sequences). The alignment was thus passed through the structure prediction module of AF2 to arrive at the PDB formatted atomic coordinates of Atg11. Docking of Atg11 with post-translationally modified hexapeptide Spc72 was performed using implicit solvation and the Rosetta force-field (*MinMover* module (Chaudhury, Lyskov, & Gray, 2010)) to obtain energy-minimized complexes. From an ensemble of 100 possible binding conformations, the modal pose was chosen which exhibited the lowest static-structure binding enthalpy.

Construction of yeast strains

ATG11 deletion was carried out by one-step gene replacement (Gietz & Schiestl, 2007), having a 40-bp homology region using HR34 and HR35 primer pairs having *HPH* marker providing resistance against hygromycin B amplified from pAG32. *ATG11* deletion in F2351 strain (Manzano-Lopez et al., 2019), with Kar9-GFP and Spc72-mCherry tagged, was carried out using HR34 and HR35 primer pairs having *HPH* marker providing resistance against hygromycin B amplified from pAG32. The *ATG11* deletion was confirmed by 5' and 3' junction primers (HR36 and HR37).

Double deletion mutants were obtained either by transforming the above *ATG11* deletion cassette in single deletion mutant background or by crossing a single deletion mutant in *MAT*a mating background having a G418 marker with *atg11*Δ cells in *MATα* (BY4742) background having *HPH* selection. The diploid cells were sporulated and after digestion of the cell wall and vortexing, the cells were plated first on YPD with hygromycin. Growing colonies were patched on G418 and colonies growing on both the selection plates were mated again with both *MAT*a (BY4741) and *MATα* (BY4742) to differentiate between haploid and diploid cells. Cells showing shmoo formation with only one mating type were taken forward for the assays.

For *atg11*Δ complementation, a ~3.9 kb fragment comprising the upstream and full-length sequence of *ATG11* was fused with a ~800 bp of *HIS3* fragment with its promoter having a 40-bp homology sequence of *ATG11* at its 3' end. The purified PCR product was transformed in the *atg11*Δ cells and the transformants were screened using HR116 and HR117 primers.

Construction of strain expressing GFP-Tub1 and Spc42-mCherry under its native promoter

To study the dynamics of microtubules, tubulin was tagged with GFP using the plasmid, pAFS125 (Straight, Marshall, Sedat, & Murray, 1997). To visualize SPBs, Spc42, a component of the central plaque of SPB, was tagged with mCherry using the primers HR142 and HR143.

Construction of *MAD2* and *BUB2* deletion strain

MAD2 deletion was carried out by one-step gene replacement (Gietz & Schiestl, 2007), having a 40-bp homology region using HR52 and HR53 primer pairs having *HPH* marker providing resistance against hygromycin B amplified from pAG32. The deletion strain was confirmed by 5' and 3' junction primers (HR66 and HR67). Similarly, *BUB2* deletion was carried out having 40-bp homology region using HR202 and HR203 primer pairs having *HPH* marker providing resistance against hygromycin B amplified from pAG32. The deletion strain was confirmed by 5' and 3' junction primers (HR206 and HR207).

Construction of strains for Bimolecular Fluorescence (BiFC) assay

We used N-terminal protein tagging vectors, pFA6a-KanMx6- p*GAL1*-VN173 and pFA6a-His3Mx6-p*GAL1*-VC155 for tagging both Atg11 and Spc72 (Sung & Huh, 2007). VN173-Atg11 and VC155-Atg11 were amplified using HR296+HR297 and HR296+HR298 primer pairs. Similarly, VN173-Spc72 and VC155-Spc72 were amplified using HR299+HR300 and HR299+HR301 primer pairs. VN-tagged fragments having G418 selection and VC-tagged fragments with *HIS3* selection were transformed into BY4741 and BY4742 backgrounds respectively. The haploid colonies obtained were mated and selected on G418 plates without histidine to obtain diploid cells expressing both fragments of the fluorophore. The control diploid cells expressing either VN-Spc72 or VC-Atg11 co-expressing Spc42-mCherry were generated by mating BY4741 expressing VN-Spc72 with BY4742 and BY4742 expressing VC-Atg11 with BY4741.

Stability of monocentric plasmid

The *atg1*Δ, *atg6*Δ, *atg11*Δ, *atg15*Δ, *atg17*Δ, *ctf19*Δ, and the isogenic wild-type strains were transformed with pRS313, a mono centromeric plasmid, and selected on a dropout media lacking histidine (SD-his) (Sikorski & Hieter, 1989). The transformants were then inoculated in a non-selective media, YPD, and allowed to grow for 7-10 generations, followed by plating dilutions to obtain single colonies. The single colonies were subsequently patched onto SD-his (selective) and YPD (non-selective) media. The mitotic stability was calculated by the number of colonies that were able to grow on selective media (SD-his) divided by the total number of colonies on non-selective media (YPD).

Chromosome loss assay

The chromosome loss assay was performed in a strain harbouring an extra non-essential chromosome that carries *SUP11* that suppresses *ade2* mutation in the assay strain, YMH58a as previously described (Hieter, Mann, Snyder, & Davis, 1985). Cells retaining this extra chromosome grow as a white-coloured colony, as the cells bypass *ade2* mutation. Loss of extra chromosome leads to the red-pigmented colony, similar to *ade2* mutant phenotype, implying loss of *SUP11* (Hieter et al., 1985). A single white colony of wild-type, *atg11*Δ, and *ctf19*Δ cells were grown in non-selective media (YPD) for 5-7 generations, both at 30°C and 37°C. The cells were plated on YPD. The number of colonies showing chromosome loss at the first division was scored for each condition in three independent biological experiments.

Flow cytometry

The overnight grown cells were inoculated to 0.2 OD_{600} the next day in YPD and were grown for 3 h. The cells were arrested at metaphase in presence of 15 µg mL^{-1} nocodazole and samples were collected from 0-6 h. After 3 h, another 15 µg mL^{-1} nocodazole was added to maintain the arrest. The cells were washed with RNase buffer (0.2 M Tris pH-7.5, 20 mM EDTA) and resuspended in 100 µL RNase buffer. The cells were treated with 10 µL of RNase A (10 mg mL^{-1}) overnight at 37°C. Cells were washed with 1x PBS and were finally resuspended in 400 µL 1x PBS and incubated overnight at 4°C. Cells were stained with propidium iodide (0.06 µg $µL^{-1}$) for 30 min in dark conditions, just before the data acquisition. Data from 30, 000 singlet cells per transformant were collected using BD FACSAria™ III and analyzed using FlowJo_V10 software. The experiments were repeated thrice using freshly grown cultures.

***In vivo* assay for kinetochore integrity: *CEN* transcriptional read-through assay**

The *CEN* transcription read-through assay was done by using a reporter plasmid containing a *GAL1-10* promoter that initiates transcription of an actin-lacZ fusion gene. A wild-type centromere inserted in the actin intron inactivates the segregational function of the *CEN*. The transcriptional block created by the *CEN* DNA-protein complex is relaxed in putative kinetochore mutants which allows transcription read-through activity from the reporter plasmid. The reporter plasmid pAKD06+*CEN4* contains a β-galactosidase reporter gene with the selectable marker *URA3*. The construct is designed to direct the integration of the reporter via homologous recombination to the *ura3* locus on chromosome V of *S. cerevisiae.* The transformants were obtained on SD-ura media. The single colony was inoculated in 5 mL of synthetic media lacking uracil, containing 2% galactose and 0.3% raffinose and was grown to OD_{600}=1. The cell pellet was washed with water and resuspended in 1 mL of Z-buffer (60 mM Na_2HPO_4, 40 mM $NaH_2PO_4.2H_2O$, 10 mM KCl, 5 mM β-ME). 0.1 mL of this was taken for the determination of OD_{610}. 0.1 mL of Z-buffer was added to the remaining 0.9 mL of cells. The cells were then permeabilized by adding 50 µL of 0.1% SDS and 100 µL of chloroform (incubated at 30°C for 15 min). 0.2 mL of 4 mg mL^{-1} ONPG (ortho-nitrophenyl-β-galactoside) was added to the cell suspension and incubated at 30°C till yellow colour developed. The reaction was stopped by adding 0.5 mL of 1 M Na_2CO_3. Cells were spun down at 10,000 g and the clear supernatant was transferred to a fresh tube. The optical density of this solution was measured at 420 and 550 nm. The enzyme activity was normalized with respect to cell density. Units of β galactosidase were measured as:

$$\text{Miller units} = \frac{1000\,[(OD_{420})-1.75\times(OD_{550})]}{t \times v \times OD_{610}}$$

t= time of reaction (min)

v= volume of cell suspension used in the assay (mL)

Live-cell imaging

Wild-type and *atg11*Δ cells tagged with GFP-Tub1 (spindle) for microtubule dynamics were grown overnight in YPD medium and re-inoculated in YPD at 0.2 OD_{600} for 3 h. The cells were pelleted at 3,000 g for 2 min. The cells were placed on a glass slide having a 2% agarose pad supplemented with 2% dextrose and the pad was sealed with a coverslip. Live-cell microscopy was performed using the Zeiss Axio Observer 7, equipped with Definite Focus. 2, Colibri 7 (LED source), TempController 2000-2 (PECON), a Plan-Apochromat 100x/1.40 oil DIC M27, EMCCD camera.

Live-cell imaging at 37°C was performed on an inverted confocal microscope (ZEISS, LSM880) equipped with a temperature-control chamber (Pecon incubator, XL multiSL), a Plan Apochromat 100x NA oil 1.4 objective and GaAsp photodetectors. For time-lapse microscopy, images were captured at a 5 min interval with 5% intensity exposure with 0.5 µm Z-steps using 488 nm and 587 nm for GFP and mCherry as excitation wavelength. All the images displayed were maximum intensity projections of images for each time using ImageJ.

Microscopic image acquisition and processing

Wild-type and deletion mutants tagged either GFP-Tub1 (spindle) or Spc42-mCherry (SPB marker) were grown overnight in YPD medium and re-inoculated in YPD at 0.2 OD_{600} for 3 h at 30°C. The cells were pelleted at 3,000 *g*. The cells were mounted on a glass slide having a 2% agarose pad supplemented with 2% dextrose and the pad was sealed with a coverslip. Large-budded (budding index of >0.6) cells of each strain were imaged using an inverted microscope (ZEISS, Axio Observer.Z1/7), a Plan-Apochromat 100x/1.40 oil DIC M27. The filters used were GFP/FITC 488, mCherry 561 for excitation, GFP/FITC 500/550 bandpass or GFP 495/500 and mCherry 565/650 or mCherry 580/750 bandpass for emission. Z-stacks at an interval of 0.5 µm were taken and maximum intensity projection for each image using ImageJ was projected.

For figures 2A-B, 2D-H, 3D-F, 4A-C, 4I-J and supporting figures S2A-E, S3B-D and S3G-H were imaged using an inverted confocal microscope (ZEISS, LSM880) equipped with an Airyscan module, 63x Plan Apochromat 1.4 NA. Z stacks were obtained at an interval of 1 µM, 488/516 and 561/595 nm excitation/emission wavelengths were used for GFP and mCherry respectively. For supporting figures S3E-F, the images were deconvoluted using the default programme with the ZEN Blue software (Zeiss).

Bimolecular Fluorescence (BiFC) assay

The overnight growing cells simultaneously expressing Spc72 fused to the N-terminal half of Venus and Atg11 tagged to the C-terminal half of the same fluorophore, were reinoculated to 0.2 OD_{600} in YEP containing 2% galactose (YPG) for 3 h. At 2 h, FM4-64 was added at a concentration of 7.5 µM for 30 min. The cells were washed twice with 1x PBS and further incubated for 1 h in YPG before microscopy.

Staining protocols

Vacuoles were visualized by staining with 7-amino-4-chloromethylcoumarin (CMAC) (ThermoFischer Scientific, Cat. No. C2110; CellTrackerTM Blue CMAC dye) dissolved in DMSO to give a 10 mM stock. Briefly, the cells were incubated with 10 μM dye at 30°C for 1 h 30 min. The cells were washed with 1× PBS thrice with 5 min incubation each and were imaged.

FM4-64 staining was performed to visualize the vacuolar membrane. Briefly, FM4-64 (ThermoFischer Scientific; Cat. No. T3166) was added at a concentration of 7.5 μM for 30 min. The cells were washed twice with 1x PBS and further incubated for 1 h in YPD before microscopy.

Nuclei were visualized by diamidino-2-phenylindole (DAPI) (ThermoFischer Scientific; Cat. No. 62248) staining. Briefly, the cells were fixed in 3.7% formaldehyde for 10 min. The cells were washed and treated with 0.05% Triton X-100 for 5 min. The cells were resuspended in 1x PBS and stained with 5 ng mL^{-1} DAPI for 10 min and imaged.

Yeast two-hybrid assays

The full-length *ATG11* (~3534 bp), *SPC72* (~1869 bp), and *CNM67* (~1746 bp) were PCR amplified and cloned in frame with the Gal4 activation/ DNA binding domain in pGADC1 and pGBDC1 respectively at BamHI and SalI sites using oligos listed in Supplementary file 2. Yeast-two hybrid analyses were performed in the strain PJ69-4A as described previously (James, Halladay, & Craig, 1996). Briefly, bait and prey plasmids were co-transformed into the *S. cerevisiae* strain PJ69-4A. Positive interactions were scored by the appearance of white-coloured colonies on a synthetic defined medium containing 6 μg mL^{-1} adenine and/ or by the growth in presence of 2 mM 3-Amino-1,2,4-triazole (3-AT) (A8056, Sigma).

Atg11 point mutants, L867G, D1001A and L1005G were constructed by overlap PCR. Briefly, PCR fragments were amplified using the primer sets HR131/RA155 and RA154/HR132 (*ATG11*-L867G) or HR131/RA153 and RA152/HR132 (*ATG11*-D1001A) or HR131/RA151 and RA150/HR132 (*ATG11*-L1005G). The equimolar ratio of the two fragments was mixed and amplified with the primer set HR131/HR132 to obtain the mutant *ATG11* ORF. The fused fragment was cloned in frame with the DNA binding domain in pGBDC1 at the BamHI and SalI sites. The clones were confirmed by restriction analysis and Sanger sequencing. Yeast two-hybrid analysis was performed as described above with the Atg11 point mutants and Spc72.

Post-acquisition analysis

Spindle length was measured by tracking it using a straight line, and freehand (for bent spindle) tool in ImageJ after maximum intensity projection for each image. Spindle orientation was measured on images that were maximum intensity projected using the angle tool in ImageJ. The angle was calculated by measuring the smaller of the two angles that the spindle forms intersecting the mother-bud axis of the cell. The astral microtubules were measured after maximum intensity projection of the images using either a straight line or a freehand tool in ImageJ. The budding index was represented as the ratio of the diameter of the daughter cell to the diameter of the mother cell. Throughout the manuscript, large-budded cells with a budding index of >0.6 are taken into consideration for all the analyses (Saunders, Hornack, Lengyel, & Deng, 1997). Statistical analyses were done using GraphPad Prism 8.4.0 software. Student's *t*-test followed by Unpaired *t*-test for comparing two groups. The data sets represented as bar graphs were analyzed using either One-way ANOVA or two-way ANOVA for multiple groups and have been mentioned in the figure legends where applicable. Scatter plots with data from three independent biological repeats were plotted as SuperPlots (Lord, Velle, Mullins, & Fritz-Laylin, 2020), displaying individual colour-coded data. The statistical analyses were done with three independent biological replicates.

Acknowledgements

We thank J. Heitman, L. Sreekumar, S. Sridhar, V. Yadav, and K. Guin for the critical reading of the manuscript. We thank D. J. Klionsky, C. Kraft, S. K. Ghosh, S. Bhattacharyya, F. Monje-Casas for sharing yeast strains and vectors, and G. Dey and S. Palani for the valuable comments. We thank N. Nala for his assistance with flow cytometry and B. Suma and K. Jayaram at the imaging facility at JNCASR. Financial support from the DBT-RA Program in Biotechnology and Life Sciences is gratefully acknowledged by MHR. The award of JC Bose Fellowship (JCB/2020/000021), SERB, and JNCASR intramural funding support to KS is acknowledged. This work was also supported by the Department of Biotechnology (DBT) grant in Life Science Research, Education and Training at JNCASR (BT/INF/22/SP27679/2018) to KS and RM and SERB grant (CRG/2019/004892) to RM. JV was supported by intramural financial support from JNCASR. RA is supported by intramural financial support from JNCASR. We also thank the members of the Molecular Mycology Laboratory for their valuable inputs and comments. Some images were created with BioRender.com.

Author Contributions

K.S. conceived the idea; M.H.R. and K.S. designed experiments; M.H.R. performed the majority of the experiments; J.V. performed the initial screen of autophagy mutants involved in chromosome segregation, stability of monocentric plasmid and *CEN* transcriptional read-through assay; R.A. created all the haploid strains used in the BiFC assay and created point mutants along with their yeast-two hybrid assay; R.C. constructed the protein network and predicted protein structure. M.H.R., J.V., R.A., and R.C. contributed new reagents/analytical tools; M.H.R., R.A., J.V., and K.S. analyzed the data; M.H.R., R.A., R.M. and K.S. wrote the paper; K.S. gathesred majority of the funding and supervised the work.

Declaration of Interests

The authors declare no competing interests.

References

Alexandru, G., Zachariae, W., Schleiffer, A., & Nasmyth, K. (1999). Sister chromatid separation and chromosome re-duplication are regulated by different mechanisms in response to spindle damage. *EMBO J, 18*(10), 2707-2721. doi:10.1093/emboj/18.10.2707

Bardin, A. J., Visintin, R., & Amon, A. (2000). A mechanism for coupling exit from mitosis to partitioning of the nucleus. *Cell, 102*(1), 21-31. doi:10.1016/s0092-8674(00)00007-6

Beach, D. L., Thibodeaux, J., Maddox, P., Yeh, E., & Bloom, K. (2000). The role of the proteins Kar9 and Myo2 in orienting the mitotic spindle of budding yeast. *Curr Biol, 10*(23), 1497-1506. doi:10.1016/s0960-9822(00)00837-x

Bloecher, A., Venturi, G. M., & Tatchell, K. (2000). Anaphase spindle position is monitored by the *BUB2* checkpoint. *Nat Cell Biol, 2*(8), 556-558. doi:10.1038/35019601

Brachat, A., Kilmartin, J. V., Wach, A., & Philippsen, P. (1998). *Saccharomyces cerevisiae* cells with defective spindle pole body outer plaques accomplish nuclear migration via half-bridge-organized microtubules. *Mol Biol Cell, 9*(5), 977-991. doi:10.1091/mbc.9.5.977

Byers, B. (1981). Cytology of the yeast life cycle. *Cold Spring Harbor Monograph Archive, 11*, 59-96.

Caydasi, A. K., Ibrahim, B., & Pereira, G. (2010). Monitoring spindle orientation: Spindle position checkpoint in charge. *Cell Div, 5*, 28. doi:10.1186/1747-1028-5-28

Chaudhury, S., Lyskov, S., & Gray, J. J. (2010). PyRosetta: a script-based interface for implementing molecular modeling algorithms using Rosetta. *Bioinformatics, 26*(5), 689-691. doi:10.1093/bioinformatics/btq007

Chen, X. P., Yin, H., & Huffaker, T. C. (1998). The yeast spindle pole body component Spc72p interacts with Stu2p and is required for proper microtubule assembly. *J Cell Biol, 141*(5), 1169-1179. doi:10.1083/jcb.141.5.1169

Cheng, J., Turkel, N., Hemati, N., Fuller, M. T., Hunt, A. J., & Yamashita, Y. M. (2008). Centrosome misorientation reduces stem cell division during ageing. *Nature, 456*(7222), 599-604. doi:10.1038/nature07386

Chowdhury, R., Allan, M. F., & Maranas, C. D. (2018). OptMAVEn-2.0: De novo design of variable antibody regions against targeted antigen epitopes. *Antibodies, 7*(3), 23. doi:10.3390/antib7030023

Cottingham, F. R., & Hoyt, M. A. (1997). Mitotic spindle positioning in *Saccharomyces cerevisiae* is accomplished by antagonistically acting microtubule motor proteins. *J Cell Biol, 138*(5), 1041-1053. doi:10.1083/jcb.138.5.1041

De Souza, C. P., & Osmani, S. A. (2007). Mitosis, not just open or closed. *Eukaryot Cell, 6*(9), 1521-1527. doi:10.1128/EC.00178-07

DeZwaan, T. M., Ellingson, E., Pellman, D., & Roof, D. M. (1997). Kinesin-related *KIP3* of *Saccharomyces cerevisiae* is required for a distinct step in nuclear migration. *J Cell Biol, 138*(5), 1023-1040. doi:10.1083/jcb.138.5.1023

Diaz-Horta, O., Sirmaci, A., Doherty, D., Nance, W., Arnos, K., Pandya, A., & Tekin, M. (2012). GPSM2 mutations in Chudley-McCullough syndrome. *Am J Med Genet A, 158A*(11), 2972-2973. doi:10.1002/ajmg.a.35636

Doherty, D., Chudley, A. E., Coghlan, G., Ishak, G. E., Innes, A. M., Lemire, E. G., . . . Zelinski, T. (2012). GPSM2 mutations cause the brain malformations and hearing loss in Chudley-McCullough syndrome. *Am J Hum Genet, 90*(6), 1088-1093. doi:10.1016/j.ajhg.2012.04.008

Dotiwala, F., Eapen, V. V., Harrison, J. C., Arbel-Eden, A., Ranade, V., Yoshida, S., & Haber, J. E. (2013). DNA damage checkpoint triggers autophagy to regulate the initiation of anaphase. *Proc Natl Acad Sci U S A, 110*(1), E41-49. doi:10.1073/pnas.1218065109

Farre, J. C., Manjithaya, R., Mathewson, R. D., & Subramani, S. (2008). PpAtg30 tags peroxisomes for turnover by selective autophagy. *Dev Cell, 14*(3), 365-376. doi:10.1016/j.devcel.2007.12.011

Fischer, E., Legue, E., Doyen, A., Nato, F., Nicolas, J. F., Torres, V., . . . Pontoglio, M. (2006). Defective planar cell polarity in polycystic kidney disease. *Nat Genet, 38*(1), 21-23. doi:10.1038/ng1701

Fraschini, R., Formenti, E., Lucchini, G., & Piatti, S. (1999). Budding yeast Bub2 is localized at spindle pole bodies and activates the mitotic checkpoint via a different pathway from Mad2. *J Cell Biol, 145*(5), 979-991. doi:10.1083/jcb.145.5.979

Fremont, S., Gerard, A., Galloux, M., Janvier, K., Karess, R. E., & Berlioz-Torrent, C. (2013). Beclin-1 is required for chromosome congression and proper outer kinetochore assembly. *EMBO Rep, 14*(4), 364-372. doi:10.1038/embor.2013.23

Fu, J., Hagan, I. M., & Glover, D. M. (2015). The centrosome and its duplication cycle. *Cold Spring Harb Perspect Biol, 7*(2), a015800. doi:10.1101/cshperspect.a015800

Geymonat, M., Peng, Q., Guo, Z., Yu, Z., Unruh, J. R., Jaspersen, S. L., & Segal, M. (2020). Orderly assembly underpinning built-in asymmetry in the yeast centrosome duplication cycle requires cyclin-dependent kinase. *eLife, 9*. doi:10.7554/eLife.59222

Gietz, R. D., & Schiestl, R. H. (2007). High-efficiency yeast transformation using the LiAc/SS carrier DNA/PEG method. *Nature Protoc, 2*, 31. doi:10.1038/nprot.2007.13

Heath, I. B. (1980). Variant mitoses in lower eukaryotes: indicators of the evolution of mitosis. *Int Rev Cytol, 64*, 1-80. doi:10.1016/s0074-7696(08)60235-1

Hieter, P., Mann, C., Snyder, M., & Davis, R. W. (1985). Mitotic stability of yeast chromosomes: a colony color assay that measures nondisjunction and chromosome loss. *Cell, 40*(2), 381-392. doi:0092-8674(85)90152-7 [pii]

10.1016/0092-8674(85)90152-7

Hoepfner, D., Schaerer, F., Brachat, A., Wach, A., & Philippsen, P. (2002). Reorientation of mispositioned spindles in short astral microtubule mutant spc72Delta is dependent on spindle pole body outer plaque and Kar3 motor protein. *Mol Biol Cell, 13*(4), 1366-1380. doi:10.1091/mbc.01-07-0338

Hotz, M., Leisner, C., Chen, D., Manatschal, C., Wegleiter, T., Ouellet, J., . . . Barral, Y. (2012). Spindle pole bodies exploit the mitotic exit network in metaphase to drive their age-dependent segregation. *Cell, 148*(5), 958-972. doi:10.1016/j.cell.2012.01.041

Hu, F., Wang, Y., Liu, D., Li, Y., Qin, J., & Elledge, S. J. (2001). Regulation of the Bub2/Bfa1 GAP complex by Cdc5 and cell cycle checkpoints. *Cell, 107*(5), 655-665. doi:10.1016/s0092-8674(01)00580-3

James, P., Halladay, J., & Craig, E. A. (1996). Genomic libraries and a host strain designed for highly efficient two-hybrid selection in yeast. *Genetics, 144*(4), 1425-1436.

Jiang, P., & Mizushima, N. (2014). Autophagy and human diseases. *Cell Res, 24*(1), 69-79. doi:10.1038/cr.2013.161

Juanes, M. A., Twyman, H., Tunnacliffe, E., Guo, Z., ten Hoopen, R., & Segal, M. (2013). Spindle pole body history intrinsically links pole identity with asymmetric fate in budding yeast. *Curr Biol, 23*(14), 1310-1319. doi:10.1016/j.cub.2013.05.057

Jumper, J., Evans, R., Pritzel, A., Green, T., Figurnov, M., Ronneberger, O., . . . Hassabis, D. (2021). Highly accurate protein structure prediction with AlphaFold. *Nature, 596*(7873), 583-589. doi:10.1038/s41586-021-03819-2

Kim, J., Kamada, Y., Stromhaug, P. E., Guan, J., Hefner-Gravink, A., Baba, M., . . . Klionsky, D. J. (2001). Cvt9/Gsa9 functions in sequestering selective cytosolic cargo destined for the vacuole. *J Cell Biol, 153*(2), 381-396. doi:10.1083/jcb.153.2.381

Knoblich, J. A. (2010). Asymmetric cell division: recent developments and their implications for tumour biology. *Nat Rev Mol Cell Biol, 11*(12), 849-860. doi:10.1038/nrm3010

Knop, M., & Schiebel, E. (1998). Receptors determine the cellular localization of a gamma-tubulin complex and thereby the site of microtubule formation. *EMBO J, 17*(14), 3952-3967. doi:10.1093/emboj/17.14.3952

Korinek, W. S., Copeland, M. J., Chaudhuri, A., & Chant, J. (2000). Molecular linkage underlying microtubule orientation toward cortical sites in yeast. *Science, 287*(5461), 2257-2259. doi:10.1126/science.287.5461.2257

Kosco, K. A., Pearson, C. G., Maddox, P. S., Wang, P. J., Adams, I. R., Salmon, E. D., . . . Huffaker, T. C. (2001). Control of microtubule dynamics by Stu2p is essential for spindle orientation and metaphase chromosome alignment in yeast. *Mol Biol Cell, 12*(9), 2870-2880. doi:10.1091/mbc.12.9.2870

Kozakov, D., Hall, D. R., Xia, B., Porter, K. A., Padhorny, D., Yueh, C., . . . Vajda, S. (2017). The ClusPro web server for protein-protein docking. *Nat Protoc, 12*(2), 255-278. doi:10.1038/nprot.2016.169

Krick, R., Muehe, Y., Prick, T., Bremer, S., Schlotterhose, P., Eskelinen, E. L., . . . Thumm, M. (2008). Piecemeal microautophagy of the nucleus requires the core macroautophagy genes. *Mol Biol Cell, 19*(10), 4492-4505. doi:10.1091/mbc.E08-04-0363

Lancaster, M. A., & Knoblich, J. A. (2012). Spindle orientation in mammalian cerebral cortical development. *Curr Opin Neurobiol, 22*(5), 737-746. doi:10.1016/j.conb.2012.04.003

Lara-Gonzalez, P., Pines, J., & Desai, A. (2021). Spindle assembly checkpoint activation and silencing at kinetochores. *Semin Cell Dev Biol, 117*, 86-98. doi:10.1016/j.semcdb.2021.06.009

Lechler, T., & Mapelli, M. (2021). Spindle positioning and its impact on vertebrate tissue architecture and cell fate. *Nat Rev Mol Cell Biol, 22*(10), 691-708. doi:10.1038/s41580-021-00384-4

Lee, C. W., Wilfling, F., Ronchi, P., Allegretti, M., Mosalaganti, S., Jentsch, S., . . . Pfander, B. (2020). Selective autophagy degrades nuclear pore complexes. *Nat Cell Biol, 22*(2), 159-166. doi:10.1038/s41556-019-0459-2

Lee, L., Tirnauer, J. S., Li, J., Schuyler, S. C., Liu, J. Y., & Pellman, D. (2000). Positioning of the mitotic spindle by a cortical-microtubule capture mechanism. *Science, 287*(5461), 2260-2262. doi:10.1126/science.287.5461.2260

Lengefeld, J., & Barral, Y. (2018). Asymmetric segregation of aged spindle pole bodies during cell division: Mechanisms and relevance beyond budding yeast? *Bioessays, 40*(8), e1800038. doi:10.1002/bies.201800038

Li, G., & Moore, J. K. (2020). Microtubule dynamics at low temperature: evidence that tubulin recycling limits assembly. *Mol Biol Cell, 31*(11), 1154-1166. doi:10.1091/mbc.E19-11-0634

Liakopoulos, D., Kusch, J., Grava, S., Vogel, J., & Barral, Y. (2003). Asymmetric loading of Kar9 onto spindle poles and microtubules ensures proper spindle alignment. *Cell, 112*(4), 561-574. doi:10.1016/s0092-8674(03)00119-3

Lord, S. J., Velle, K. B., Mullins, R. D., & Fritz-Laylin, L. K. (2020). SuperPlots: Communicating reproducibility and variability in cell biology. *Journal of Cell Biology, 219*(6). doi:10.1083/jcb.202001064

Maekawa, H., Neuner, A., Ruthnick, D., Schiebel, E., Pereira, G., & Kaneko, Y. (2017). Polo-like kinase Cdc5 regulates Spc72 recruitment to spindle pole body in the methylotrophic yeast *Ogataea polymorpha*. *eLife, 6*. doi:10.7554/eLife.24340

Manzano-Lopez, J., Matellan, L., Alvarez-Llamas, A., Blanco-Mira, J. C., & Monje-Casas, F. (2019). Asymmetric inheritance of spindle microtubule-organizing centres preserves replicative lifespan. *Nat Cell Biol, 21*(8), 952-965. doi:10.1038/s41556-019-0364-8

Mao, K., Wang, K., Liu, X., & Klionsky, D. J. (2013). The scaffold protein Atg11 recruits fission machinery to drive selective mitochondria degradation by autophagy. *Dev Cell, 26*(1), 9-18. doi:10.1016/j.devcel.2013.05.024

Markus, S. M., Kalutkiewicz, K. A., & Lee, W. L. (2012). Astral microtubule asymmetry provides directional cues for spindle positioning in budding yeast. *Exp Cell Res, 318*(12), 1400-1406. doi:10.1016/j.yexcr.2012.04.006

Matellan, L., Manzano-Lopez, J., & Monje-Casas, F. (2020). Polo-like kinase acts as a molecular timer that safeguards the asymmetric fate of spindle microtubule-organizing centers. *eLife, 9*. doi:10.7554/eLife.61488

Matscheko, N., Mayrhofer, P., Rao, Y., Beier, V., & Wollert, T. (2019). Atg11 tethers Atg9 vesicles to initiate selective autophagy. *PLoS Biol, 17*(7), e3000377. doi:10.1371/journal.pbio.3000377

Matsui, A., Kamada, Y., & Matsuura, A. (2013). The role of autophagy in genome stability through suppression of abnormal mitosis under starvation. *PLoS Genet, 9*(1), e1003245. doi:10.1371/journal.pgen.1003245

Miller, R. K., Cheng, S. C., & Rose, M. D. (2000). Bim1p/Yeb1p mediates the Kar9p-dependent cortical attachment of cytoplasmic microtubules. *Mol Biol Cell, 11*(9), 2949-2959. doi:10.1091/mbc.11.9.2949

Miller, R. K., & Rose, M. D. (1998). Kar9p is a novel cortical protein required for cytoplasmic microtubule orientation in yeast. *J Cell Biol, 140*(2), 377-390. doi:10.1083/jcb.140.2.377

Mizushima, N., & Levine, B. (2020). Autophagy in human diseases. *N Engl J Med, 383*(16), 1564-1576. doi:10.1056/NEJMra2022774

Molk, J. N., Schuyler, S. C., Liu, J. Y., Evans, J. G., Salmon, E. D., Pellman, D., & Bloom, K. (2004). The differential roles of budding yeast Tem1p, Cdc15p, and Bub2p protein dynamics in mitotic exit. *Mol Biol Cell, 15*(4), 1519-1532. doi:10.1091/mbc.e03-09-0708

Moore, J. K., D'Silva, S., & Miller, R. K. (2006). The CLIP-170 homologue Bik1p promotes the phosphorylation and asymmetric localization of Kar9p. *Mol Biol Cell, 17*(1), 178-191. doi:10.1091/mbc.e05-06-0565

Morrow, A., Underwood, J., Seldin, L., Hinnant, T., & Lechler, T. (2019). Regulated spindle orientation buffers tissue growth in the epidermis. *eLife, 8*. doi:10.7554/eLife.48482

Musacchio, A., & Salmon, E. D. (2007). The spindle-assembly checkpoint in space and time. *Nat Rev Mol Cell Biol, 8*(5), 379-393. doi:10.1038/nrm2163

Nelson, S. A., Sanson, A. M., Park, H. O., & Cooper, J. A. (2012). A novel role for the GTPase-activating protein Bud2 in the spindle position checkpoint. *PLoS One, 7*(4), e36127. doi:10.1371/journal.pone.0036127

Palmer, R. E., Sullivan, D. S., Huffaker, T., & Koshland, D. (1992). Role of astral microtubules and actin in spindle orientation and migration in the budding yeast, *Saccharomyces cerevisiae*. *J Cell Biol, 119*(3), 583-593. doi:10.1083/jcb.119.3.583

Pereira, G., Hofken, T., Grindlay, J., Manson, C., & Schiebel, E. (2000). The Bub2p spindle checkpoint links nuclear migration with mitotic exit. *Mol Cell, 6*(1), 1-10.

Pereira, G., Tanaka, T. U., Nasmyth, K., & Schiebel, E. (2001). Modes of spindle pole body inheritance and segregation of the Bfa1p-Bub2p checkpoint protein complex. *EMBO J, 20*(22), 6359-6370. doi:10.1093/emboj/20.22.6359

Ro, H. S., Song, S., & Lee, K. S. (2002). Bfa1 can regulate Tem1 function independently of Bub2 in the mitotic exit network of *Saccharomyces cerevisiae*. *Proc Natl Acad Sci U S A, 99*(8), 5436-5441. doi:10.1073/pnas.062059999

Saunders, W., Hornack, D., Lengyel, V., & Deng, C. (1997). The *Saccharomyces cerevisiae* kinesin-related motor Kar3p acts at preanaphase spindle poles to limit the number and length of cytoplasmic microtubules. *J Cell Biol, 137*(2), 417-431. doi:10.1083/jcb.137.2.417

Segal, M., & Bloom, K. (2001). Control of spindle polarity and orientation in *Saccharomyces cerevisiae*. *Trends Cell Biol, 11*(4), 160-166. doi:10.1016/s0962-8924(01)01954-7

Shaw, S. L., Yeh, E., Maddox, P., Salmon, E. D., & Bloom, K. (1997). Astral microtubule dynamics in yeast: a microtubule-based searching mechanism for spindle orientation and nuclear migration into the bud. *J Cell Biol, 139*(4), 985-994. doi:10.1083/jcb.139.4.985

Shcheprova, Z., Baldi, S., Frei, S. B., Gonnet, G., & Barral, Y. (2008). A mechanism for asymmetric segregation of age during yeast budding. *Nature, 454*(7205), 728-734. doi:10.1038/nature07212

Shintani, T., Huang, W. P., Stromhaug, P. E., & Klionsky, D. J. (2002). Mechanism of cargo selection in the cytoplasm to vacuole targeting pathway. *Dev Cell, 3*(6), 825-837. doi:10.1016/s1534-5807(02)00373-8

Sikorski, R. S., & Hieter, P. (1989). A system of shuttle vectors and yeast host strains designed for efficient manipulation of DNA in *Saccharomyces cerevisiae*. *Genetics, 122*(1), 19-27. doi:10.1093/genetics/122.1.19

Soues, S., & Adams, I. R. (1998). *SPC72*: a spindle pole component required for spindle orientation in the yeast *Saccharomyces cerevisiae*. *J Cell Sci, 111 (Pt 18)*, 2809-2818.

Sreekumar, L., Kumari, K., Guin, K., Bakshi, A., Varshney, N., Thimmappa, B. C., . . . Sanyal, K. (2021). Orc4 spatiotemporally stabilizes centromeric chromatin. *Genome Res, 31*(4), 607-621. doi:10.1101/gr.265900.120

Stark, C., Breitkreutz, B. J., Reguly, T., Boucher, L., Breitkreutz, A., & Tyers, M. (2006). BioGRID: a general repository for interaction datasets. *Nucleic Acids Res, 34*(Database issue), D535-539. doi:10.1093/nar/gkj109

Steinegger, M., & Soding, J. (2017). MMseqs2 enables sensitive protein sequence searching for the analysis of massive data sets. *Nat Biotechnol, 35*(11), 1026-1028. doi:10.1038/nbt.3988

Straight, A. F., Marshall, W. F., Sedat, J. W., & Murray, A. W. (1997). Mitosis in living budding yeast: anaphase A but no metaphase plate. *Science, 277*(5325), 574-578. doi:10.1126/science.277.5325.574

Strome, E. D., Wu, X., Kimmel, M., & Plon, S. E. (2008). Heterozygous screen in *Saccharomyces cerevisiae* identifies dosage-sensitive genes that affect chromosome stability. *Genetics, 178*(3), 1193-1207. doi:10.1534/genetics.107.084103

Sullivan, D. S., & Huffaker, T. C. (1992). Astral microtubules are not required for anaphase B in *Saccharomyces cerevisiae*. *J Cell Biol, 119*(2), 379-388. doi:10.1083/jcb.119.2.379

Sung, M. K., & Huh, W. K. (2007). Bimolecular fluorescence complementation analysis system for *in vivo* detection of protein-protein interaction in *Saccharomyces cerevisiae*. *Yeast, 24*(9), 767-775. doi:10.1002/yea.1504

Thakur, J., & Sanyal, K. (2012). A coordinated interdependent protein circuitry stabilizes the kinetochore ensemble to protect CENP-A in the human pathogenic yeast *Candida albicans*. *PLoS Genet, 8*(4), e1002661. doi:10.1371/journal.pgen.1002661

Tirnauer, J. S., O'Toole, E., Berrueta, L., Bierer, B. E., & Pellman, D. (1999). Yeast Bim1p promotes the G1-specific dynamics of microtubules. *J Cell Biol, 145*(5), 993-1007. doi:10.1083/jcb.145.5.993

Varma, D., Chandrasekaran, S., Sundin, L. J., Reidy, K. T., Wan, X., Chasse, D. A., . . . Cook, J. G. (2012). Recruitment of the human Cdt1 replication licensing protein by the loop domain of Hec1 is required for stable kinetochore-microtubule attachment. *Nat Cell Biol, 14*(6), 593-603. doi:10.1038/ncb2489

Vessoni, A. T., Filippi-Chiela, E. C., Menck, C. F., & Lenz, G. (2013). Autophagy and genomic integrity. *Cell Death Differ, 20*(11), 1444-1454. doi:cdd2013103 [pii]

10.1038/cdd.2013.103

Wang, Y., Hu, F., & Elledge, S. J. (2000). The Bfa1/Bub2 GAP complex comprises a universal checkpoint required to prevent mitotic exit. *Curr Biol, 10*(21), 1379-1382. doi:10.1016/s0960-9822(00)00779-x

Wang, Y., Zhang, X., Zhang, H., Lu, Y., Huang, H., Dong, X., . . . Jiang, T. (2012). Coiled-coil networking shapes cell molecular machinery. *Mol Biol Cell, 23*(19), 3911-3922. doi:10.1091/mbc.E12-05-0396

Yamashita, Y. M., Mahowald, A. P., Perlin, J. R., & Fuller, M. T. (2007). Asymmetric inheritance of mother versus daughter centrosome in stem cell division. *Science, 315*(5811), 518-521. doi:10.1126/science.1134910

Yao, W., Li, Y., Wu, L., Wu, C., Zhang, Y., Liu, J., . . . Yi, C. (2020). Atg11 is required for initiation of glucose starvation-induced autophagy. *Autophagy, 16*(12), 2206-2218. doi:10.1080/15548627.2020.1719724

Yeh, E., Skibbens, R. V., Cheng, J. W., Salmon, E. D., & Bloom, K. (1995). Spindle dynamics and cell cycle regulation of dynein in the budding yeast, *Saccharomyces cerevisiae*. *J Cell Biol, 130*(3), 687-700. doi:10.1083/jcb.130.3.687

Yin, H., Pruyne, D., Huffaker, T. C., & Bretscher, A. (2000). Myosin V orientates the mitotic spindle in yeast. *Nature, 406*(6799), 1013-1015. doi:10.1038/35023024

Yorimitsu, T., & Klionsky, D. J. (2005). Atg11 links cargo to the vesicle-forming machinery in the cytoplasm to vacuole targeting pathway. *Mol Biol Cell, 16*(4), 1593-1605. doi:10.1091/mbc.e04-11-1035

Zimdahl, B., Ito, T., Blevins, A., Bajaj, J., Konuma, T., Weeks, J., . . . Reya, T. (2014). Lis1 regulates asymmetric division in hematopoietic stem cells and in leukemia. *Nat Genet, 46*(3), 245-252. doi:10.1038/ng.2889